Substrate Specificity and Kinetic Studies of PADs 1, 3, and 4 Identify Potent and Selective Inhibitors of Protein Arginine Deiminase 3[†]

Bryan Knuckley,[‡] Corey P. Causey,[‡] Justin E. Jones,[‡] Monica Bhatia,[‡] Christina J. Dreyton,[‡] Tanesha C. Osborne,[‡] Hidenari Takahara,[§] and Paul R. Thompson*,[‡]

[‡]*Department of Chemistry and Biochemistry, University of South Carolina, 631 Sumter Street, Columbia, South Carolina 29208, and* [§]*Department of Applied Bioresource Sciences, School of Agriculture, Ibaraki University, 21-1 Chuou 3, Ami, Inashiki, Ibaraki 3000393, Japan*

ABSTRACT: Protein citrullination has been shown to regulate numerous physiological pathways (e.g., the innate immune response and gene transcription) and is, when dysregulated, known to be associated with numerous human diseases, including cancer, rheumatoid arthritis, and multiple sclerosis. This modification, also termed deimination, is catalyzed by a group of enzymes called the protein arginine deiminases (PADs). In mammals, there are five PAD family members (i.e., PADs 1, 2, 3, 4, and 6) that exhibit tissue-specific expression patterns and vary in their subcellular localization. The kinetic characterization of PAD4 was recently reported, and these efforts guided the development of the two most potent PAD4 inhibitors (i.e., F- and Cl-amidine) known to date. In addition to being potent PAD4 inhibitors, we show here that Cl-amidine also exhibits a strong inhibitory effect against PADs 1 and 3, thus indicating its utility as a pan PAD inhibitor. Given the increasing number of diseases in which dysregulated PAD activity has been implicated, the development of PAD-selective inhibitors is of paramount importance. To aid that goal, we characterized the catalytic mechanism and substrate specificity of PADs 1 and 3. Herein, we report the results of these studies, which suggest that, like PAD4, PADs 1 and 3 employ a reverse protonation mechanism. Additionally, the substrate specificity studies provided critical information that aided the identification of PAD3-selective inhibitors. These compounds, denoted F4- and Cl4-amidine, are the most potent PAD3 inhibitors ever described.

Aberrantly increased protein arginine deiminase (PAD)[1] activity has been associated with numerous human diseases, including rheumatoid arthritis (*1*), multiple sclerosis (*2*), Alzheimer's disease (*3*), ulcerative colitis (*4*), and numerous cancers (*5*, *6*), thereby suggesting these enzymes as novel therapeutic targets (*7*). Five PAD isozymes (i.e., PADs 1, 2, 3, 4, and 6) exist in humans, and these enzymes catalyze the posttranslational conversion of peptidylarginine to peptidylcitrulline in numerous protein substrates, e.g., histones H2A, H3, and H4, fibrinogen, keratin, and trichohyalin (Figure 1A). While there is significant evidence to suggest that PAD4 plays a causative role in the aforementioned diseases, there is also emerging evidence suggesting that other PADs, in particular PAD2, may also play a role (*8*). Significant questions regarding the contributions of PADs 1, 3, and 6 to human disease also remain unanswered; thus a greater understanding of the physiological and pathophysiological roles of these enzymes is necessary in order to define the individual contributions of these enzymes to human disease and normal human physiology.

In humans, the genes encoding the five PAD isozymes are all clustered on chromosome 1 (1p35−36), and this genomic organization is conserved among mammals. Each isozyme is also highly conserved at the amino acid sequence level (70−95% homology retained in mammals), with PADs 1 and 3 being the most closely related isozymes (68% AA sequence identity) (*9*, *10*). Deiminated proteins have been identified throughout mammalian tissues, and the resulting reduction in net positive charge can potentially have dramatic effects on protein folding and protein−protein interactions (*11*, *12*).

To date, PAD4 has been the focus of many biochemical studies (*1*, *10*, *13−15*), thus making it the best characterized PAD. For example, this isozyme has been shown to regulate chromatin structure and function through its ability to deiminate histones H2A, H3, and H4, as well as p300 (*12*, *14−18*). Putative roles for PAD4 in apoptosis, and in the formation of neutrophil extracellular traps (NETs), have also been described (*19−24*). The prominent role of PAD4 in transcriptional regulation, as well as its role in RA, prompted our efforts to design and synthesize two highly potent mechanism-based inhibitors that are denoted F- and Cl-amidine (Figure 1B) (*7*, *19*, *25*). These compounds irreversibly inactivated PAD4 by covalently modifying an active site cysteine (Cys645) that is critical for catalysis. Inactivation likely proceeds via an initial attack of the Cys645 thiolate on the iminium carbon of the haloacetamidine warhead, resulting in the formation of a tetrahedral intermediate. His471 then likely donates a proton to stabilize this intermediate, thereby promoting halide displacement by the sulfur atom. The resultant three-membered sulfonium

*To whom correspondence should be addressed at the Department of Chemistry, The Scripps Research Institute, Scripps Florida, 130 Scripps Way, Jupiter, FL 33458. Tel: (561) 228-2860. Fax: (561) 228-3050. E-mail: Pthompso@scripps.edu.

[1]Abbreviations: PAD, protein arginine deiminase; Cit, citrulline; RA, rheumatoid arthritis; BAEE, benzoyl-ʟ-arginine ethyl ester; BAA, benzoyl-ʟ-arginine amide; BAME, benzoyl-ʟ-arginine methyl ester; DTT, dithiothreitol; TCEP, tris(2-carboxyethyl)phosphine; EDTA, ethylenediaminetetraacetic acid.
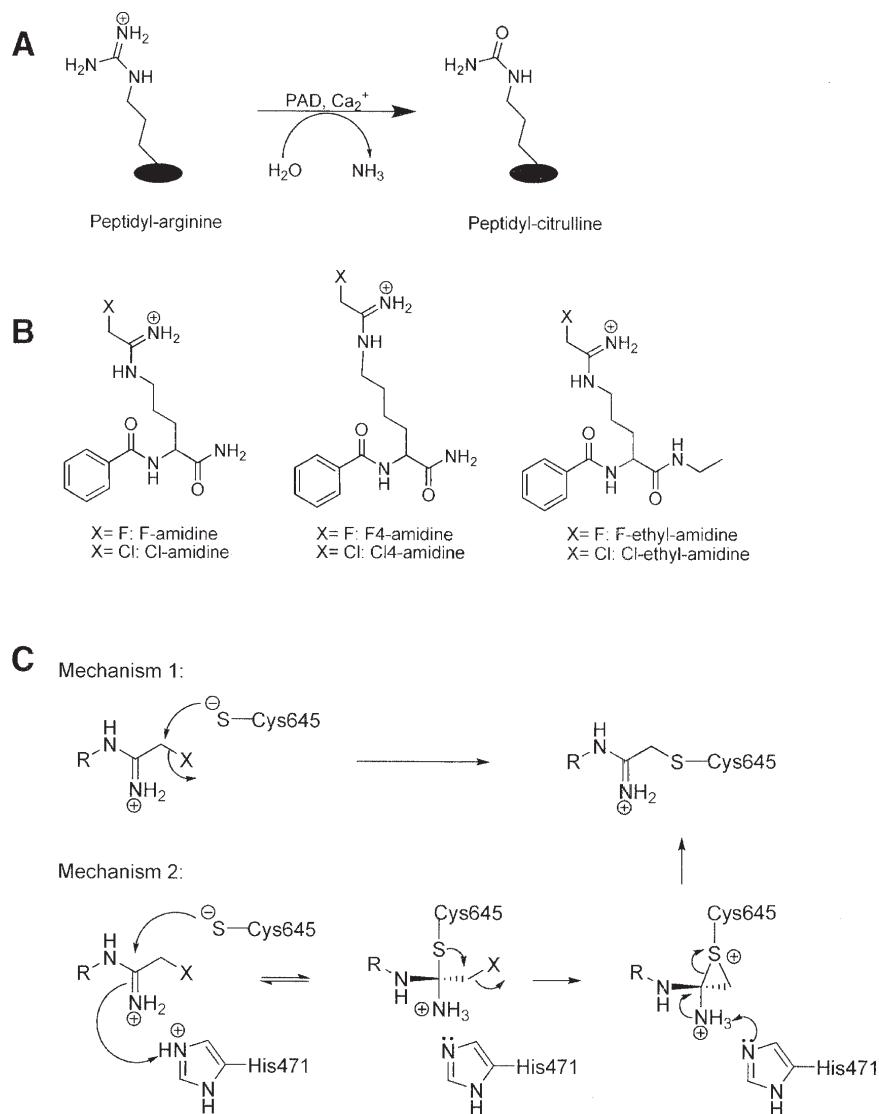
FIGURE 1: (A) PADs catalyze the posttranslational conversion of peptidylarginine to peptidylcitrulline. (B) Structures of PAD inhibitors including F- and Cl-amidine, F4- and Cl4-amidine, and F- and Cl-ethylamidine. (C) Proposed mechanism of PAD inactivation.

ring then collapses to form a thioether adduct, rendering the enzyme inactive (Figure 1C) (*19*, *25*, *26*).

Unlike PAD4, little is known about the physiological roles of the remaining PADs, although it has been speculated that PADs 1, 2, and 3 play an important role in skin homeostasis and moisturization. Consistent with this hypothesis is the fact that PAD1 is expressed throughout the epidermis and that PADs 2 and 3 are expressed in the spinous and granular layer, respectively (*27*, *28*). In addition to these roles, PAD3 is also believed to play an important role in hair follicle formation due to its ability to deiminate trichohyalin, an abundant, arginine-rich (22.7%), structural protein present in the inner root sheath and medulla of hair follicles (*28*, *29*). Given the presumed roles of PAD activity in normal skin moisturization, dysregulation of these enzymes has been suggested to play a causative role in psoriasis, an autoimmune disorder that causes red, scaly patches to form on the skin (*27*, *29*, *30*). The fact that vitamin D derivatives are known to induce the expression of PADs 1, 2, and 3 in keratinocytes, and are used to treat this disease (*29*, *31*), suggests that decreased PAD activity is associated with psoriasis.

These and other studies demonstrate the importance of understanding the roles that PADs 1 and 3 play in skin moisturization and hair follicle differentiation. Additionally, their potential roles in these processes suggest that inhibition of these enzymes could lead to a number of undesired side effects. Therefore, in an effort to guide the design of isozyme-specific PAD inhibitors, we initiated studies to both characterize the catalytic mechanism of PADs 1 and 3 and identify important substrate recognition elements. Herein, we describe the results of these studies. Specifically, we demonstrate that Cl-amidine is a pan PAD inhibitor. Additionally, the results of pH profiles and pK_a measurements on the active site Cys demonstrate that PADs 1 and 3, like PAD4, utilize a reverse protonation mechanism. Furthermore, the substrate specificities of PADs 1, 3, and 4 were probed by determining steady-state kinetic parameters for both small synthetic substrates and various peptides. The results of these studies identified isozyme-specific differences that led to the discovery of the PAD3-specific inhibitors F4- and Cl4-amidine; these compounds are the most potent PAD3 inhibitors described to date.

MATERIALS AND METHODS

Chemicals. Dithiothreitol (DTT), *N*-α-benzoyl ʟ-arginine ethyl ester (BAEE), citrulline, β-mercaptoethanol, Triton X-100, imidazole, protease inhibitor cocktail (catalog no. P8465), and tris(2-carboxyethyl)phosphine (TCEP) were acquired from Sigma

Table 1: Histone Peptide Derivatives

peptide	sequence
AcH4−21	1-Ac-SGRGKGGKGLGKGGAKRHRKV
AcH4−18	1-Ac-SGRGKGGKGLGKGGAKRH
AcH4−16	1-Ac-SGRGKGGKGLGKGGAK
AcH4−15	1-Ac-SGRGKGGKGLGKGGA
AcH4−13	1-Ac-SGRGKGGKGLGKG
AcH4−5	1-Ac-SGRGK
AcH4−5 S1A	1-Ac-**A**GRGK
AcH4−5 G2A	1−Ac-S**A**RGK
AcH4−5 G4A	1-Ac-SGR**A**K
AcH4−5 K5A	1-Ac-SGRG**A**
AcH4−21 N(1)	2-Ac-GRGKGGKGLGKGGAK
AcH4−21 N(2)	3-Ac-RGKGGKGLGKGGAK
AcH4−21 K16A	1-Ac-SGRGKGGKGLGKGGA**A**RHRKV
AcH4−21 K20A	1-Ac-SGRGKGGKGLGKGGAKRHR**A**V
AcH4−21 R3A	1-Ac-SG**A**GKGGKGLGKGGAKRHRAV
AcH4−21 R17A	1-Ac-SGRGKGGKGLGKGGAK**A**HRAV
AcH4−21 R19A	1-Ac-SGRGKGGKGLGKGGAKRH**A**AV
AcH4−21 R17,19K	1-Ac-SGRGKGGKGLGKGGAK**K**H**K**AV
AcH4−21 all Ac−K	1-Ac-SGRG**K**^{Ac}GG**K**^{Ac}GLG**K**^{Ac}GGA**K**^{Ac}RHR**K**^{Ac}V

Aldrich (St. Louis, MO). N-α-Benzoyl-L-arginine methyl ester (BAME) and N-G-methyl-L-arginine acetate (MMA) were obtained from MP Biomedicals (Irvine, CA). N-α-Benzoyl-L-arginine (BA) and N-α-benzoyl-L-arginine amide (BAA) were obtained from Acros (Hampton, NH). The synthesis of a subset of the peptides listed in Table 1 has been previously described (*32*). The AcH4−21 R3A, AcH4−21 R17A, and AcH4−21 R19A peptides were synthesized on the solid phase using the Fmoc strategy and purified by reverse-phase liquid chromatography. The synthesis of F- and Cl-amidine, as well as F4- and Cl4-amidine, has previously been described (*19, 25, 33*).

Synthesis of N-α-Benzoyl-N^5-(tert-butoxycarbonyl)-L-ornithine Ethyl Amide. N-α-Benzoyl-N^5-(*tert*-butoxycarbonyl)-L-ornithine (200 mg, 0.59 mmol), S-(1-oxido-2-pyridyl)-N,N,N',N'-tetramethylthiouronium hexafluorophosphate (HOTT) (330 mg, 0.89 mmol), and triethylamine (0.17 mL, 1.2 mmol) were dissolved in dry DMF (2 mL) and allowed to stir at room temperature. After 10 min, ethylamine (0.6 mL of a 2 M solution in THF, 1.2 mmol) was added, and stirring was allowed to continue at room temperature. After 45 min, the reaction was partitioned between EtOAc (15 mL) and brine (30 mL). The organics were separated, and the aqueous layer was extracted twice more with EtOAc. The organics were combined, washed with 2 M HCl (2 × 15 mL), H_2O (2 × 15 mL), saturated $NaHCO_3$ (2 × 15 mL), H_2O (3 × 15 mL), and brine (15 mL), dried over $MgSO_4$, and concentrated under vacuum to yield the product as a white powder (167 mg, 78%). ^{1}H NMR (400 MHz, $CDCl_3$) δ (ppm): 7.76 (d, $J = 7.2$ Hz, 2H), 7.42−7.3 (m, 4 H), 7.05 (br, 1H), 4.86 (t, $J = 6$ Hz, 1H), 4.8−4.73 (m, 1H), 3.33−3.14 (m, 3H), 2.98−3.08 (m, 1H), 1.8−1.76 (m, 1H), 1.76−1.65 (m, 1H), 1.56−1.47 (m, 2H), 1.35 (s, 9H). ^{13}C NMR (100 MHz, $CDCl_3$) δ (ppm): 171.84, 167.48, 156.58, 133.84, 131.70, 128.49, 127.19, 79.18, 52.33, 39.29, 34.40, 30.38, 28.40, 26.53, 14.66. HRMS ($C_{19}H_{30}N_3O_4^+$): calcd 364.2236, observed 364.2240.

Synthesis of N-α-Benzoyl-L-ornithine Ethyl Amide. Cold TFA (10 mL) was added to N-α-benzoyl-N^5-(*tert*-butoxycarbonyl)-L-ornithine ethyl amide (166 mg, 0.46 mmol), and the reaction was stirred at 0 °C. After 30 min, the reaction was allowed to warm to room temperature and stir for an additional 30 min. The TFA was removed under a stream of nitrogen. The remaining residue was dissolved in H_2O (20 mL), extracted with ether (2 × 5 mL), and lyophilized to yield the product as a clear

hygroscopic solid (162 mg, 94%). ^{1}H NMR (400 MHz, D_2O) δ (ppm): 7.51 (d, $J = 8$ Hz, 2H), 7.37−7.22 (m, 3H), 4.27 (dd, $J = 2, 8$ Hz, 1H), 2.97 (q, $J = 7.2$ Hz, 2H), 2.78 (t, $J = 7.6$ Hz, 2H), 1.75−1.45 (m, 4H), 0.84 (t, $J = 7.2$ Hz, 3H). ^{13}C NMR (100 MHz, D_2O) δ (ppm): 172.90, 170.77, 132.58, 132.30, 128.56, 127.08, 53.99, 38.69, 34.35, 27.85, 23.28, 13.32. HRMS ($C_{14}H_{22}N_3O_2^+$): calcd 264.1712, observed 264.1711.

Synthesis of Cl-ethylamidine. N-α-Benzoyl-L-ornithine ethyl amide (38 mg, 0.1 mmol) and ethyl chloroacetimidate (HCl) (28.2 mg, 0.2 mmol) were dissolved in dry methanol (3 mL). Cs_2CO_3 (48.8 mg, 0.15 mmol) was added, and the reaction was stirred at room temperature. After 16 h, the reaction was quenched with TFA and purified by RP-HPLC to yield the product as a white powder. ^{1}H NMR (400 MHz, D_2O) δ (ppm): 7.60−7.57 (m, 2H), 7.45−7.39 (m, 1H), 7.35−7.29 (m, 2H), 4.22 (dd, $J = 2, 8$ Hz, 1H), 4.19 (s, 2H), 3.18 (t, $J = 6.8$ Hz, 2H), 3.03 (q, $J = 7.2$ Hz, 2H), 1.82−1.45 (m, 4H), 0.90 (t, $J = 7.2$ Hz, 3H). ^{13}C NMR (100 MHz, D_2O) δ (ppm): 173.07, 170.92, 162.68, 132.68, 132.36, 128.63, 127.13, 54.12, 41.82, 38.94, 34.38, 28.08, 23.03, 13.40. HRMS ($C_{16}H_{24}ClN_4O_2^+$): calcd 339.1588, observed 339.1593.

Synthesis of F-ethylamidine. N-α-Benzoyl-L-ornithine ethyl amide (30 mg, 0.08 mmol) and ethyl fluoroacetimidate (HCl) (25 mg, 0.16 mmol) were dissolved in dry methanol (3 mL). Cs_2CO_3 (39 mg, 0.12 mmol) was added, and the reaction was stirred at room temperature. After 16 h, the reaction was quenched with TFA and purified by RP-HPLC to yield the product as white powder. ^{1}H NMR (400 MHz, D_2O) δ (ppm): 7.57−7.55 (m, 2H), 7.44−7.38 (m, 1H), 7.33−7.27 (m, 2H), 5.05 (d, $J_{H-F} = 44.8$ Hz, 2H), 4.21 (dd, $J = 2.4, 8$ Hz, 1H), 3.18 (t, $J = 6.8$ Hz, 2H), 3.01 (q, $J = 7.2$ Hz, 2H), 1.79−1.48 (m, 4H), 0.88 (t, $J = 7.2$ Hz, 3H). ^{13}C NMR (100 MHz, D_2O) δ (ppm): 173.10, 170.92, 162.47 (d, $J_{C-F} = 19.9$ Hz), 132.66, 132.34, 128.61, 127.11, 77.43 (d, $J_{C-F} = 178.29$ Hz), 54.13, 41.29, 34.37, 27.83, 23.17, 13.37. HRMS ($C_{16}H_{24}FN_4O_2^+$): calcd 323.1883, observed 323.1884.

Cloning, Expression, and Purification of PADs 1 and 3. For protein expression, the genes encoding PADs 1 and 3 were cloned from the original pGEX-6P1 vector (*34*) into the pET16B vector, which contains a 6×-His tag followed by a factor Xa cleavage site. PAD1 was cloned using the following primers: forward 5′-AAAAAACATATGGCCCCAAAGAGAG-3′ and reverse 5′-AAAAAACTCGAGGGGCACCATGTTC-3′. PAD3 was cloned using the following primers: forward 5′-AAAAAA-CATATGTCGCTGCAGAGAATC-3′ and reverse 5′-AAAAAA-CTCGAGGGGCACCATGTTC-3′. The forward primers contain an *Nde*I restriction site (underlined) and either 13 base pairs or 15 base pairs that correspond to the 5′-coding region of the PAD 1 and 3 genes, respectively. The reverse primers contain an *Xho*I restriction site (underlined) followed by 13 base pairs that correspond to the 3′-coding region of the PAD 1 and 3 genes. The resulting pET16b-PAD1 and pET16b-PAD3 constructs were sequenced to ensure that no mutations were incorporated during PCR amplification. PADs 1 and 3 were purified analogously to previously described methods (*35*). Although the His-tagged proteins were recovered in modest yield (1.0−1.5 mg/L), this procedure, in one step, afforded PADs 1 and 3 in greater than 95% purity (Supporting Information Figure S1). A detailed description of the purification protocol can be found in the Supporting Information.

Citrulline Production Assay. After a 10 min preincubation period at 37 °C, either PAD 1 or 3 was added to assay buffer (60 μL total volume; 10 mM $CaCl_2$, 50 mM NaCl, 100 mM Tris-HCl, pH 7.6, 2 mM DTT) plus 10 mM BAEE to initiate the reaction.

Following the addition of enzyme, the reaction was allowed to proceed for 10 min and then flash frozen in liquid nitrogen. Citrulline production was then quantified using previously established methods (*32*, *36*, *37*). PAD activity was linear with respect to time and enzyme concentration.

Ammonia Production Assay. The amount of ammonia produced as a function of time was determined by preincubating assay buffer containing 10 mM BAEE at 37 °C for 10 min before adding 0.2 μM enzyme (PAD 1 or 3) to start the reaction. At specific time points (0, 2, 4, 6, 10, 15 min), 60 μL of the reaction was removed and quenched by flash freezing. In order to quantify ammonia production, 180 μL of 50 mM EDTA was added to the quenched reaction, and the method of Sugawara and Oyama was used to measure the amount of ammonia produced (*38*).

Calcium Dependence. Varying concentrations of calcium (0−10 mM) were incubated in 50 mM NaCl, 2 mM DTT, 10 mM BAEE, and 100 mM Tris-HCl, pH 7.6. Reactions were preincubated at 37 °C for 10 min before the addition of 0.2 μM enzyme (PAD 1 or 3). The reactions were allowed to proceed for 10 min and then flash frozen in liquid nitrogen. Citrulline production was determined as described above, and the data were fit to eq 1

$$v/V_{max} = [Ca^{2+}]^n/(K_D + [Ca^{2+}]^n) \tag{1}$$

using GraFit version 5.0.11 (*39*). K_D is the dissociation constant and n is the Hill coefficient. Note that for these assays PADs 1 and 3 were dialyzed into EDTA-free long-term storage buffer (20 mM Tris-HCl, pH 8.0, 2 mM DTT or 250 μM TCEP, 500 mM NaCl, and 10% glycerol).

Substrate Specificity Studies. The steady-state kinetic parameters were determined for peptide substrates and synthetic arginine substrates using the methodology described above. Briefly, assay buffer containing various concentrations of substrate was preincubated at 37 °C for 10 min prior to the addition of either PAD 1, 3, or 4 (0.2 μM). The reaction was allowed to proceed for 15 min (peptides) or 10 min (arginine derivatives) before freezing in liquid nitrogen. Citrulline formation was measured using the methodology described above. Peptide substrates were dissolved in 50 mM HEPES, pH 8.0. The initial rates obtained from these experiments were fit to eq 2

$$v = V_{max}[S]/(K_m + [S]) \tag{2}$$

using Grafit 5.0.1.1 (*39*).

pH Profiles. pH profiles for PADs 1 and 3 were generated by measuring the steady-state kinetic parameters for the deimination of BAEE over the pH range 6.0−9.5. Stock concentrations of BAEE were prepared in 50 mM buffer at the desired pH. Reaction mixtures containing 50 mM NaCl, 2 mM DTT, 100 mM buffer (Bis-tris, pH 6.5−7, or Tris-HCl, pH 7−9.5), 10 mM CaCl$_2$, and BAEE at various concentrations (0−10 mM in a final volume of 60 μL) were preincubated for 10 min prior to the addition of either PAD 1 or 3. The initial rates obtained from these experiments were fit to eq 2 using GraFit version 5.0.11 (*39*). The k_{cat} and k_{cat}/K_m values obtained from this analysis were plotted as a function of pH and fit to eq 3

$$\log[y_{obs}] = \log(y_{max}/(1 + 10^{pK_{a1} - pH} + 10^{pH - pK_{a2}})) \tag{3}$$

using GraFit version 5.0.11 (*39*). y_{max} is the amount of activity at the pH optimum.

Inactivation Studies. Inactivation reactions containing 10 mM CaCl$_2$ and 100 mM of buffer (pH 6−8.5 Tris-HCl) were incubated with 2.0 μM PAD1 at 37 °C for 10 min before adding either iodoacetamide or 2-chloroacetamidine (dissolved in 50 mM buffer) to initiate the reaction (60 μL final volume). At various time points (0−30 min), an aliquot (6 μL) was removed and added to assay buffer, which was preincubated for 10 min at 37 °C to measure residual PAD1 activity (60 μL total volume). Reactions were allowed to proceed for 15 min before being flash frozen in liquid nitrogen. Citrulline production was measured according to the methodology described above, and the residual activity data, thus obtained, were fit to eq 4

$$v = v_0 e^{-kt} \tag{4}$$

using Grafit 5.0.1.1 (*39*). v is the velocity, v_0 is the initial velocity, k is the pseudo-first-order rate constant for inactivation, and t is time. Due to a lack of inactivator saturation, second-order rate constants for enzyme inactivation, k_{inact}/K_I, were determined by plotting the observed inactivation rates (k_{obs}) versus inactivator concentration and fitting the data to eq 5

$$k_{obs} = (k_{inact}/K_I)[I] \tag{5}$$

using Grafit 5.0.1.1 (*39*). k_{inact} is the maximal rate of inactivation, K_I is the concentration of inactivator that yields half-maximal inactivation, and [I] is the concentration of inactivator. The slopes thus obtained, i.e., k_{inact}/K_I, were plotted versus pH and subsequently fit to eq 6

$$y = ((y_{min} + y_{max}) \times 10^{pH - pK_a})/(10^{pH - pK_a} + 1) \tag{6}$$

using GraFit version 5.0.11 (*39*). Y_{min} is the minimum rate, and y_{max} is the maximum rate.

IC$_{50}$ Values. IC$_{50}$ values were measured as previously described for PAD4 (*19*, *33*). The data were fit to eq 7

$$\text{fractional activity of PAD} = 1/(1 + [I]/IC_{50}) \tag{7}$$

using Grafit 5.0.1.1 (*39*).

RESULTS AND DISCUSSION

PADs 1 and 3 Produce Ammonia and Citrulline in Equimolar Amounts. Previous studies have established that PAD4 uses a hydrolytic mechanism to produce ammonia and peptidylcitrulline in equimolar amounts (*40*). To confirm that citrulline and ammonia are also the major products of the PAD 1 and 3 catalyzed reactions, experiments to measure the formation of these products were undertaken. As described previously (*32*), these experiments were performed because the central thiouronium intermediate can be hydrolyzed to form one of several different products, including citrulline plus ammonia or urea and ornithine. The results of these experiments demonstrated that, like PAD4, PADs 1 and 3 produce equimolar amounts of citrulline and ammonia (Supporting Information Figure S2). Thus, PADs 1 and 3 are *bona fide* PADs.

Calcium Dependence. PADs are known to be calcium-dependent enzymes; therefore, the concentration dependence of calcium activation for PADs 1 and 3 was determined using BAEE as the substrate. The sigmoidal nature of the curve indicates that calcium activates these enzymes in a cooperative fashion. For both enzymes, the concentration of calcium required for half-maximal activity, that is, the $K_{0.5}$, is in the mid to high micromolar range (Table 2). The fact that the Hill coefficients are greater than 1 for both enzymes at the pH optimum indicates that multiple calcium ions are required to efficiently activate these enzymes. These data are consistent with previously reported

Table 2: Calcium Dependence of PADs 1 and 3 with BAEE[a]

	pH	$K_{0.5}$ (μM)[b]	n[c]
PAD1	6.0	550 ± 40	5.0 ± 3.6
	7.6	140 ± 90	1.4 ± 0.6
	9.0	400 ± 50	3.2 ± 1.1
PAD3	6.0	950 ± 110	3.7 ± 1.1
	7.6	550 ± 80	2.2 ± 0.8
	8.5	1500 ± 1100	1.0 ± 0.4

[a]Values were determined in duplicate by incubating the enzyme with BAEE at 37 °C. [b]$K_{0.5}$ is the concentration of calcium that yields half-maximal activity. [c]n is the Hill coefficient.

values for these isozymes (*41−43*) as well as PAD4 (*32*). The requirement for multiple calcium ions is also consistent with the structure of the PAD4·calcium complex, which shows that this enzyme binds to up to five calcium ions at sites distal from the active site. Additional studies (not shown) demonstrated that calcium activates these enzymes by ≥10000-fold, similarly to PAD4.

We also determined whether or not other cations (i.e., Mg^{2+}, Mn^{2+}, Zn^{2+}, and Ba^{2+}) could substitute for calcium. With the exception of barium, little to no activity was observed with most of these cations, even after long incubation times (up to 2 h) (Supporting Information Table S1); barium, another group II metal ion, activated PADs 1 and 3 to ~15% and 2.5%, respectively, of the level of calcium. These results indicate that PADs 1 and 3, like PAD4, are highly specific for calcium. Given that supraphysiological levels of calcium are required for activity *in vitro*, typical intracellular calcium concentrations range from 100 nM to 1 μM, and given that other metal ions could not substitute for calcium, our results suggest that the PADs must be subject to an additional layer of regulation, e.g., a chaperone or posttranslational modification that decreases the amount of calcium required to activate these enzymes *in vivo*.

Steady-State Kinetic Analysis of Synthetic Arginine Derivatives. The steady-state kinetic parameters were determined for BAA, BAME, and BAEE (Table 3) (*32, 37*). BAA was identified as the best small molecule substrate for PAD1, with a k_{cat}/K_m value of 22000 $M^{-1} s^{-1}$, which is similar to the previously reported value obtained for PAD4 (*40*). The values obtained for BAME and BAEE were also comparable to those determined for PAD4, although we note that the K_m value obtained with BAME was significantly lower for PAD1 (0.37 ± 0.07 mM) than PAD4 (1.66 ± 0.26 mM). In comparison to PADs 1 and 4, all of the small molecule substrates tested are relatively poor PAD3 substrates. For example, k_{cat}/K_m values of 130, 120, and 26 $M^{-1} s^{-1}$ were obtained for BAA, BAME, and BAEE, respectively. The large decrease in k_{cat}/K_m is driven by an increase in K_m; this is best exemplified by the fact that saturation kinetics were not observed for BAEE, and thus only k_{cat}/K_m values could be determined (Table 3). These values are in agreement with previously established values (*41, 44*). For example, Mechin et al. observed a k_{cat}/K_m for BAEE of 32000 $M^{-1} s^{-1}$ (k_{cat} of 11.31 s^{-1} and K_m of 0.35 mM) for PAD1 and 230 $M^{-1} s^{-1}$ (k_{cat} of 1.73 s^{-1} and K_m of 7.50 mM) for PAD3. Similar trends have been reported by Guerrin et al. (*44*). The slight variations in k_{cat} and K_m may be due to the high temperature (55 °C) and high level of reducing agent (10 mM DTT) used in previous studies.

To better understand the molecular basis for why these benzoylated arginine derivatives are such poor PAD3 substrates, a structural model of this enzyme was generated using Swiss-Model. A comparison of this model to the previously determined

Table 3: Steady-State Kinetic Parameters for Benzoylated Arg Substrates[a]

	substrate	PAD1	PAD3	PAD4[c]
K_m (mM)	BAA	0.16 ± 0.05	13.9 ± 1.8	0.25 ± 0.06
	BAEE	0.19 ± 0.07	ND[b]	1.36 ± 0.19
	BAME	0.37 ± 0.07	10.8 ± 2.7	1.66 ± 0.26
k_{cat} (s^{-1})	BAA	3.57 ± 0.18	1.85 ± 0.15	2.76 ± 0.16
	BAEE	0.27 ± 0.02	ND	5.94 ± 0.26
	BAME	3.85 ± 0.16	1.26 ± 0.19	5.57 ± 0.28
k_{cat}/K_m ($s^{-1} M^{-1}$)	BAA	22000 ± 3600	130 ± 80	11000 ± 2700
	BAEE	1500 ± 300	25 ± 6.0	4400 ± 1400
	BAME	10400 ± 2300	120 ± 70	3300 ± 1100

[a]Kinetic parameters were measured by incubating the enzyme at 37 °C. [b]ND = not determined. [c]Values taken from Kearney et al. (*32*).

PAD4·calcium·BAA complex revealed that PAD3 lacks a residue corresponding to Arg374 in PAD4; this residue is a glycine in PAD3. As this residue has previously been shown to be important for PAD4 substrate recognition (*19, 45, 46*), by forming two key hydrogen bonds to the backbone carbonyls surrounding the site of deimination, we generated the PAD3G374R mutant to evaluate whether the lack of this residue causes the comparatively low activity of PAD3. Surprisingly, the kinetic parameters obtained with the PAD3G374R mutant, for both BAA ($K_m = 17.5 \pm 6.4$ mM, $k_{cat} = 2.1 \pm 0.6$ s^{-1}, $k_{cat}/K_m = 120$ $M^{-1} s^{-1}$) and BAEE ($k_{cat}/K_m = 13.8$ $M^{-1} s^{-1}$), are nearly identical to those obtained with the wild-type enzyme. The fact that the PAD3G374R mutant does not display PAD4-like kinetics with benzoylated arginine derivatives suggests either that this enzyme has a very different substrate specificity profile than PAD4, that the inserted Arg residue cannot be properly positioned to interact with the substrate, or, alternatively, that, in addition to its requirement for calcium, PAD3 may be subject to additional levels of regulation (e.g., interacting proteins or posttranslational modifications) that activate it toward physiologically relevant substrates.

Working Model of PAD Catalysis. Over the past few years, the conclusions of numerous crystallographic and biochemical studies have aided the construction of a working model for PAD4 catalysis (*26, 32, 47*) In this model, Cys645 acts as the active site nucleophile, and His471 is involved in general acid/base catalysis. The reaction is initiated by the nucleophilic attack of the thiolate of Cys645 on the substrate guanidinium, which gives rise to the first tetrahedral intermediate. His471 then acts as a general acid, donating a proton to the departing amine either during or after the formation of the first tetrahedral intermediate (*26*). Collapse of this intermediate results in the release of ammonia and the formation of an *S*-alkylthiouronium intermediate, the existence of which has been verified in numerous members of the guanidino group modifying enzyme family. His471 then acts as a general base to activate a water molecule for nucleophilic attack on the thiouronium intermediate. This attack results in the formation of a second tetrahedral intermediate that ultimately collapses to regenerate the enzyme and release citrulline.

Based on the proposed mechanism of catalysis, one would expect that the rates of catalysis would increase with increasing pH as the concentration of the active site thiolate increases and then fall upon deprotonation of the active site His. However, previous studies with PAD4, as well as other members of this family of enzymes (e.g., dimethylarginine diaminohydrolase (DDAH) (*48*), a number of bacterial arginine deiminases (ADIs) (*48−50*), and agmatine deiminase (J. E. Jones and P. R. Thompson, unpublished data)), have shown that the pK_a of the active site Cys is ≥8.0 and
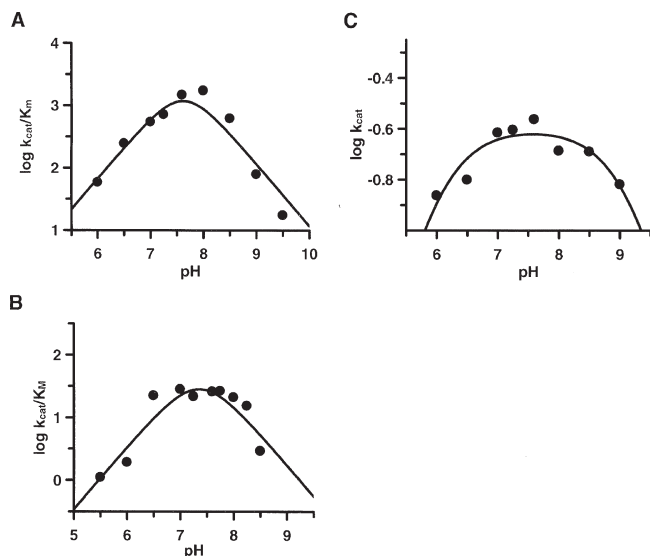
FIGURE 2: Plot of log k_{cat}/K_m versus pH for (A) PAD1 and (B) PAD3. (C) Plot of log k_{cat} versus pH for PAD1.

likely corresponds to the descending limb of the k_{cat}/K_m versus pH rate profile. Given these precedents, we set out to assess whether PADs 1 and 3 employ a similar catalytic mechanism by determining pH rate profiles for PADs 1 and 3 and by determining the pK_a of the active site Cys in PAD1 via iodoacetamide and 2-chloroacetamidine inactivation kinetics.

pH Rate Profiles. The steady-state kinetic parameters were determined for the deimination of BAEE over a range of pH values (5.5–9.0) for both PADs 1 and 3. These experiments were performed because such studies can often identify functional groups in the free enzyme (k_{cat}/K_m), ES complex (k_{cat}), and substrate (k_{cat}/K_m) that are critical for catalysis (*51*). The pH rate profiles for PADs 1 and 3 showed trends similar to those previously reported for PAD4 (*47*). For example, like PAD4, the plots of log k_{cat}/K_m versus pH, for both PADs 1 and 3, are bell-shaped, suggesting that two ionizable groups must be in the correct protonation state to facilitate substrate capture. The log k_{cat}/K_m versus pH profile for PAD1 identified a pK_a value of 7.5 ± 0.2 for the ascending limb and a pK_a of 7.6 ± 0.2 for the descending limb (Figure 2A). For PAD3 the pK_a values are 7.0 ± 0.4 and 8.2 ± 0.5 for the ascending and descending limbs, respectively (Figure 2B). Based on the architecture of the PAD active site and previous studies with PAD4, these pK_a values likely correspond to the protonation states of His471 and Cys645 (PAD4 numbering) in PADs 1 and 3. Note that for PADs 1 and 3 the pK_a values obtained from this analysis are within 3.5 pH units of one another; therefore, the actual pK_a values were calculated according to the methods of Segel (*52*) (Supporting Information Table S2).

Also like PAD4, the log k_{cat} versus pH plot for PAD1 is bell-shaped, which suggests that two active site residues must be correctly protonated for substrate turnover after the formation of the enzyme–substrate complex (ES) (Figure 2C). Note that a log k_{cat} versus pH profile could not be constructed for PAD3 because nonsaturating kinetics were observed for the deimination of BAEE. Also note that large differences in the calcium dependence of PADs 1 and 3 were not apparent over the range of pH values tested (Table 2); the observed changes in activity as a function of pH are therefore not attributable to a lack of calcium saturation. Finally, note that PAD activity was linear with respect to time at all pH values evaluated in these studies.
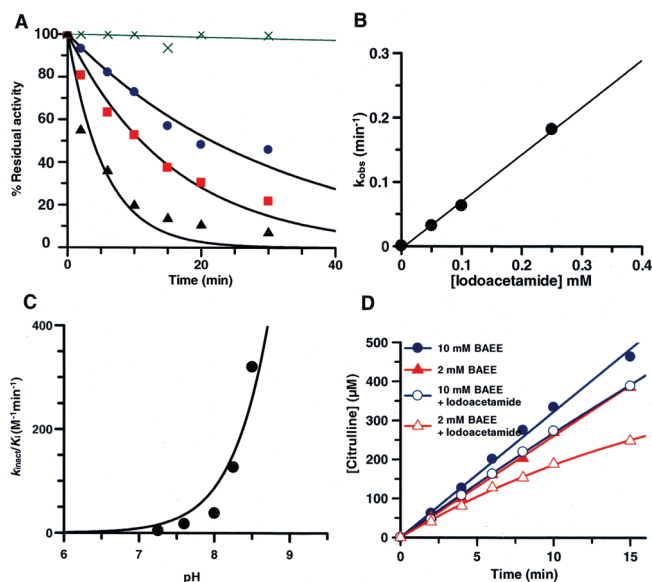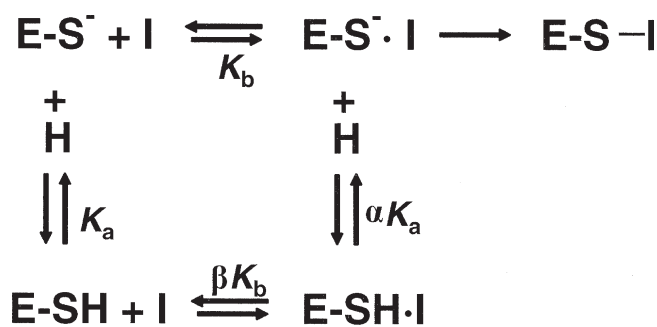

FIGURE 3: Time- and concentration-dependent inactivation of PAD1 by iodoacetamide. (A) Inactivation of PAD1 at pH 7.6 at various concentrations of iodoacetamide: (×) 0 μM, (●) 50 μM, (■) 100 μM, and (▲) 250 μM. (B) Plot of the pseudo-first-order rate constants of inactivation, i.e., k_{obs}, versus iodoacetamide concentration for PAD1 inactivation. (C) Plot of the second-order rate constants of inactivation, i.e., k_{inact}/K_I, versus pH to identify the pK_a of the active site cysteine. (D) Substrate protection experiments with PAD1 demonstrate the substrate can protect against the iodoacetamide-induced inactivation of PAD1.

Iodoacetamide Inactivation Kinetics. Iodoacetamide inactivation kinetics were next used to measure the pK_a of the active site Cys and thereby definitively assign the pK_a of this residue. Because of the similarities in the pH rate profiles obtained for PADs 1 and 3, we focused only on PAD1. For these experiments, various concentrations of iodoacetamide were incubated with PAD1, and the residual activity was measured as a function of time in order to obtain pseudo-first-order rates of inactivation, i.e., k_{obs} (Figure 3A). Subsequently, second-order inactivation rate constants, i.e., k_{inact}/K_I, were obtained at each pH by plotting the k_{obs} values versus iodoacetamide concentration (Figure 3B). The k_{inact}/K_I values were then plotted against pH. Using this analysis, a pK_a value of 8.8 ± 0.2 was determined (Figure 3C). Note that substrate protection experiments were used to show that enzyme inactivation was due to the preferential modification of an active site residue (Figure 3D).

The pK_a value obtained from this analysis is in reasonable agreement with the descending limb of the pH rate profile and likely corresponds to the pK_a of the active site cysteine of PAD1. As described above, similar results have been reported for PAD4 and other members of the guanidino group modifying enzymes (*48–50*), suggesting that a high pK_a active site Cys is a universal feature of, at least, the hydrolase branch of this enzyme superfamily. Given that the thiolate is the more reactive species, these results are counterintuitive. However, there are numerous examples in the literature of thiol-reactive enzymes that possess high pK_a values and where the pK_a assignments are the reverse of the simplest assumption (*47, 53*); these enzymes are said to employ a "reverse protonation mechanism". We have previously invoked such a mechanism for PAD4, and our data suggest that PAD1 also utilizes a reverse protonation mechanism to deiminate peptidyl arginine. Based on the similarities in the pH rate profiles, PAD3 likely employs a similar mechanism.

Scheme 1: Binding of a Positively Charged or Neutral Inactivator (I) to either the E−SH (Thiol Form of the Enzyme) or E−S⁻ (Thiolate) Form of the Enzyme

$$\text{E-S}^- + \text{I} \rightleftharpoons_{K_b} \text{E-S}^- \cdot \text{I} \longrightarrow \text{E-S} - \text{I}$$

$$+ \qquad\qquad +$$
$$\text{H} \qquad\qquad \text{H}$$

$$\Big\Updownarrow K_a \qquad\qquad \Big\Updownarrow \alpha K_a$$

$$\text{E-SH} + \text{I} \underset{\beta K_b}{\rightleftharpoons} \text{E-SH} \cdot \text{I}$$

Consistent with a reverse protonation mechanism is the fact that the decrease in the k_{cat}/K_m at the pH extremes is primarily due to an increase in K_m. A similar trend was observed for PAD4, and while changes in K_m as a function of pH can be difficult to interpret, the data imply that the substrate binds preferentially to a specific form of the enzyme at the pH optimum (*47, 52*); this form likely corresponds to a negatively charged thiolate and positively charged imidazolium ion (i.e., the ES⁻H⁺ form of the enzyme) (Scheme 1). If we make the reasonable assumption that the ascending limb of the pH profile corresponds to the pK_a of the active site His, it is apparent that only a fraction of the enzyme will exist as the thiolate and imidazolium ion, a form of the enzyme that is uniquely poised to carry out the first step of the reaction. Although speculative, the small portion of "active" enzyme may serve as a mechanism to protect the PADs from nonspecific inactivation by, for example, reactive oxygen species *in vivo*.

2-Chloroacetamidine Inactivation Kinetics. Fast and colleagues have previously suggested that thiol deprotonation occurs by a substrate-assisted mechanism; i.e., the positively charged guanidinium depresses the pK_a of the active site thiol by ~3 pH units resulting in the loss of a proton either to solvent or to an unknown base (*47, 48*) (Scheme 1). To determine if this step is obligatory, i.e., thiol deprotonation must occur after substrate binding, we determined whether a positively charged inactivator, in this case, 2-chloroacetamidine, can influence the pK_a of the active site Cys.

The methodology described above for the iodoacetamide inactivation experiments was used to obtain the pseudo-first-order and second-order rate constants of 2-chloroacetamidine-induced PAD1 inactivation (Figure 4). Plots of k_{obs} versus 2-chloroacetamidine concentration were linear over the concentration range tested (Figure 4B), and the overall plots of k_{inact}/K_I versus pH assigned a pK_a of 9.5 ± 0.2 for the active site Cys (Figure 4C). Although slightly higher than the pK_a value obtained from the iodoacetamide inactivation experiments, this pK_a value also corresponds reasonably well to the descending limb of the pH profile. Note that increasing concentrations of substrate protected against inactivation, thus indicating that inactivation by 2-chloroacetamidine was most likely due to the modification of the active site cysteine (Figure 4D). These results demonstrated that the positive charge of this inactivator does not influence k_{inact}/K_I and are, therefore, inconsistent with a mechanism that involves the obligatory binding of the inactivator to the thiol form of the enzyme prior to proton loss and enzyme inactivation, i.e., a pure substrate-assisted mechanism. Although our results favor substrate binding to the thiolate/imidazolium
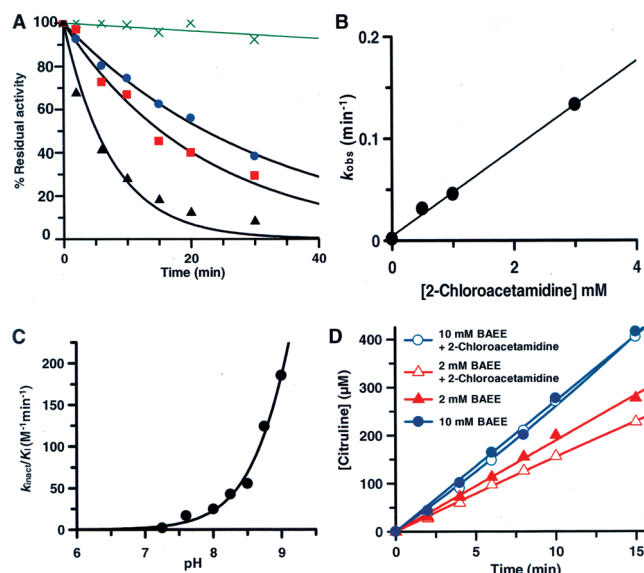

FIGURE 4: Time- and concentration-dependent inactivation of PAD1 by 2-chloroacetamidine. (A) Inactivation of PAD1 at pH 7.6 for various concentrations of 2-chloroacetamide: (×) 0 μM, (●) 500 μM, (■) 1000 μM, and (▲) 3000 μM. (B) Plot of the pseudo-first-order rate constants of inactivation, i.e., k_{obs}, versus 2-chloroacetamidine concentration for PAD1 inactivation. (C) Plot of the second-order rate constants of inactivation, i.e., k_{inact}/K_I, versus pH to identify the pK_a of the active site cysteine. (D) Substrate protection experiments with PAD1 demonstrate substrate can protect against the 2-chloroacetamidine-induced inactivation of PAD1.

form of the enzyme, they do not rule out the possibility that the substrate can bind to both the thiol and thiolate forms of the enzyme (Scheme 1), as we have previously suggested (*47*). Additionally, it is possible that at high concentrations of substrate, and at acidic pH values, binding to the thiol form of the enzyme would predominate, and under those circumstances the positive charge of the substrate would undoubtedly depress the pK_a of the active site Cys, thereby favoring its deprotonation.

Substrate Specificity Studies. Previous studies have shown that the N-termini of histones H2A, H3, and H4 are the major *in vivo*, and *in vitro*, sites of PAD4 modification (*40, 54*). To characterize the substrate specificity of PAD4, a series of peptides, based on the N-terminus of histone H4, were synthesized (Table 1). Histone H4 was chosen for these studies because PAD4 is known to deiminate this protein at arginines 3, 17, and 19 *in vitro* and R3 *in vivo* (*15, 17*) and because we have previously shown that H4 tail mimics are deiminated with comparable efficiency to the benzoylated arginine derivatives (*32*). It was expected that, by comparing the steady-state kinetic parameters obtained for these substrates with PAD4 to those obtained with PADs 1 and 3, we could identify residues surrounding the site of modification that play significant roles in substrate binding; any observed differences could then be exploited for the future design of PAD-specific inhibitors (Table 4).

To further validate the use of these peptides, the steady-state kinetic parameters were determined for histone H4 and initially compared to those obtained for BAEE. The results of these studies indicate that PADs 1 and 4 deiminate BAEE and histone H4 with roughly comparable kinetics: the k_{cat}/K_m values are only 2−3-fold higher for histone H4. A more dramatic 28-fold increase in k_{cat}/K_m was observed for PAD3, suggesting that longer range interactions are important for PAD3 substrate recognition. Notably, all three enzymes deiminate the AcH4−21

Table 4: Steady-State Kinetic Parameters for Histone-Based Peptides[a]

	PAD1			PAD3			PAD4		
peptide	k_{cat} (s^{-1})	K_m (mM)	k_{cat}/K_m (M^{-1} s^{-1})	k_{cat} (s^{-1})	K_m (mM)	k_{cat}/K_m (M^{-1} s^{-1})	k_{cat} (s^{-1})	K_m (mM)	k_{cat}/K_m (M^{-1} s^{-1})
AcH4−21	0.81 ± 0.06	0.21 ± 0.04	4000 ± 800	0.31 ± 0.07	0.42 ± 0.14	700 ± 200	3.39 ± 0.19	0.64 ± 0.12	5300 ± 1700
AcH4−18	0.64 ± 0.05	0.22 ± 0.05	3000 ± 600	4.92 ± 0.87	1.95 ± 0.49	2500 ± 800	2.29 ± 0.99	0.52 ± 0.13	4400 ± 2000
AcH4−16	0.60 ± 0.07	0.20 ± 0.05	3100 ± 800	0.08 ± 0.01	0.15 ± 0.05	500 ± 180	2.30 ± 0.16	0.59 ± 0.12	3900 ± 900
AcH4−15	0.75 ± 0.08	0.16 ± 0.04	4600 ± 1550	N/A	N/A	2000 ± 100	2.53 ± 0.15	0.58 ± 0.10	4400 ± 900
AcH4−13	N/A[b]	N/A	< 1	N/A	N/A	85 ± 25	2.83 ± 0.15	0.86 ± 0.16	3300 ± 400
AcH4−5	0.90 ± 0.12	0.33 ± 0.09	2700 ± 500	N/A	N/A	1000 ± 100	4.97 ± 0.28	0.95 ± 0.17	5200 ± 900
AcH4−5 S1A	0.59 ± 0.09	0.30 ± 0.11	2000 ± 650	0.21 ± 0.08	0.95 ± 0.63	220 ± 80	N/A	N/A	3500 ± 700
AcH4−5 G2A	1.13 ± 0.22	0.80 ± 0.29	1400 ± 300	0.62 ± 0.16	0.69 ± 0.34	900 ± 600	N/A	N/A	5800 ± 800
AcH4−5 G4A	0.98 ± 0.08	0.58 ± 0.09	1700 ± 850	N/A	N/A	80 ± 40	N/A	N/A	6600 ± 1100
AcH4−5 K5A	0.93 ± 0.16	0.37 ± 0.13	2500 ± 750	N/A	N/A	50 ± 30	N/A	N/A	16000 ± 7000
AcH4−21 N(1)	0.45 ± 0.06	0.11 ± 0.03	4200 ± 500	N/A	N/A	200 ± 20	1.04 ± 0.04	0.18 ± 0.12	5700 ± 3500
AcH4−21 N(2)	0.48 ± 0.06	0.36 ± 0.08	1400 ± 200	N/A	N/A	< 1	0.45 ± 0.06	0.32 ± 0.20	1400 ± 550
AcH4−21 K16A	0.87 ± 0.23	0.66 ± 0.28	1300 ± 400	N/A	N/A	700 ± 20	5.96 ± 0.47	0.43 ± 0.14	14000 ± 6500
AcH4−21 K20A	0.77 ± 0.13	0.34 ± 0.11	2300 ± 1900	N/A	N/A	1000 ± 40	3.27 ± 0.11	0.17 ± 0.03	19000 ± 8400
AcH4−21 R3A	1.46 ± 0.05	0.44 ± 0.07	3300 ± 800	N/A	N/A	10 ± 7	1.01 ± 0.07	1.75 ± 0.42	580 ± 40
AcH4−21 R17A	N/A	N/A	600 ± 150	N/A	N/A	300 ± 20	4.46 ± 0.17	1.70 ± 0.21	2700 ± 650
AcH4−21 R19A	1.83 ± 0.07	0.48 ± 0.04	3700 ± 400	N/A	N/A	< 1	0.86 ± 0.21	2.16 ± 0.69	400 ± 100
AcH4−21 R17,19K	0.56 ± 0.06	0.48 ± 0.06	1200 ± 150	0.34 ± 0.08	0.86 ± 0.29	400 ± 180	1.69 ± 0.34	3.27 ± 1.10	500 ± 150
AcH4−21 all Ac-K	0.57 ± 0.03	0.15 ± 0.03	3900 ± 150	1.08 ± 0.22	0.59 ± 0.21	1800 ± 1300	3.59 ± 0.21	1.07 ± 0.23	3400 ± 750
histone H4	N/A	N/A	4300 ± 900	N/A	N/A	700 ± 200	1.25 ± 0.20	0.14 ± 0.03	9000 ± 1500

[a]Kinetic parameters were measured by incubating the enzyme at 37 °C. [b]N/A = not applicable.

peptide with comparable efficiency to histone H4, thereby validating the use of histone H4-based tail mimics to probe PAD substrate specificity. To further probe the substrate specificity of PADs 1, 3, and 4, arginine substitutions were used to identify the preferred sites of modification. Additionally, the effects of peptide length, N-terminal amino acid deletions, and neighboring residues on substrate recognition were evaluated in an effort to identify specific substrate recognition elements.

Arginine Substitutions. To identify the preferred sites of modification in the H4-tail mimics, the steady-state kinetic parameters were determined for a series of arginine-substituted peptides; the sequences of these peptides are depicted in Table 1. For PAD1, the AcH4−21 R3A and R19A peptides retain similar levels of activity as the AcH4−21 peptide; that is, the k_{cat}/K_m values are 3300 and 3700 M^{-1} s^{-1}, respectively, versus 4000 M^{-1} s^{-1} for the AcH4−21 peptide. In contrast, the activity of the AcH4−21 R17A mutant peptide is reduced by greater than 5-fold (k_{cat}/K_m = 600 M^{-1} s^{-1}). These results suggest that R17 is the major site deiminated by PAD1 in the AcH4−21 peptide (Figure 5A). For PAD3, the k_{cat}/K_m values for the deimination of the AcH4−21 and AcH4−21 R17A peptides are 700 and 300 M^{-1} s^{-1}, respectively, whereas the deimination rates for the AcH4−21 R3A and R19A peptides are both reduced by more than 70-fold, suggesting that R3 and R19 are the major sites of modification by PAD3 (Figure 5A).

Consistent with previous reports for PAD4, the fact that the k_{cat}/K_m for the AcH4−21 R3A peptide is reduced by ∼10-fold (5300 to 575 M^{-1} s^{-1}) indicates that this residue is a major site of *in vitro* modification. R19 also appears to be preferentially deiminated, as the k_{cat}/K_m for the R19A "mutant" is reduced by ∼13-fold. As with PAD3, R17 appears to be a minor site of deimination as the effect of the R17A substitution was relatively minor (∼2-fold). In summary, PADs 1 and 3 appear to preferentially deiminate these H4-tail mimics at R3 and R17, whereas PAD1 preferentially modifies R17.

Effect of Peptide Length on Substrate Recognition. We next examined the effect of peptide length on substrate recognition by measuring the kinetic parameters for a series of histone

AcH4−21-based C-terminal and N-terminal deletion peptides. The results of these analyses indicate that, for PADs 1 and 4, there was little variability in the rates at which the C-terminally truncated peptides were modified (Table 4). For example, the differences in k_{cat}/K_m between the AcH4−21 peptide and shorter peptides (AcH4−16, AcH4−15, AcH4−13, and AcH4−5) are at most 2-fold, suggesting that long-range interactions play only a minimal role in substrate recognition. A less than 4-fold decrease in k_{cat}/K_m was also observed with the N-terminal deletion peptides (AcH4−21 N(1) and AcH4−21 N(2)). In total, peptide length seems to only slightly influence substrate recognition by PADs 1 and 4 (Figure 5B). In contrast, for PAD3, the k_{cat}/K_m for the AcH4−21 peptide is 5.4-fold higher than the best small molecule PAD3 substrate (i.e., BAA), again suggesting that longer range interactions are important for substrate recognition by this isozyme. Given that similarly high rates of deimination were observed with the AcH4−5 peptide, these results suggest that the residues immediately surrounding the major sites of deimination contribute the most to this effect. Consistent with this hypothesis is the fact that the increase in k_{cat}/K_m is mostly driven by a decrease in K_m.

Site-Directed "Mutagenesis". Alanine scanning "mutagenesis" was used to evaluate the specific contributions of neighboring residues to substrate recognition. First, a series of single lysine to alanine mutant peptides (i.e., AcH4−21 K16A and AcH4−21 K20A) were tested as substrates for PADs 1, 3, and 4. The results show a modest ∼3-fold increase in the deiminating activity of PAD4, as compared to the AcH4−21 peptide, suggesting that neighboring positively charged residues negatively influence the deiminating activity of PAD4. In contrast, no such trend was observed for PADs 1 or 3; that is, less than a 3-fold decrease in activity was measured for these peptides (Table 4, Figure 5C). In addition to these mutant peptides, we measured the rates of citrullination using a histone AcH4−21 peptide variant in which all of the Lys residues are acetylated; these experiments were performed because these residues are known to be acetylated *in vivo* (55). For PAD1, the results of these analyses indicate that the
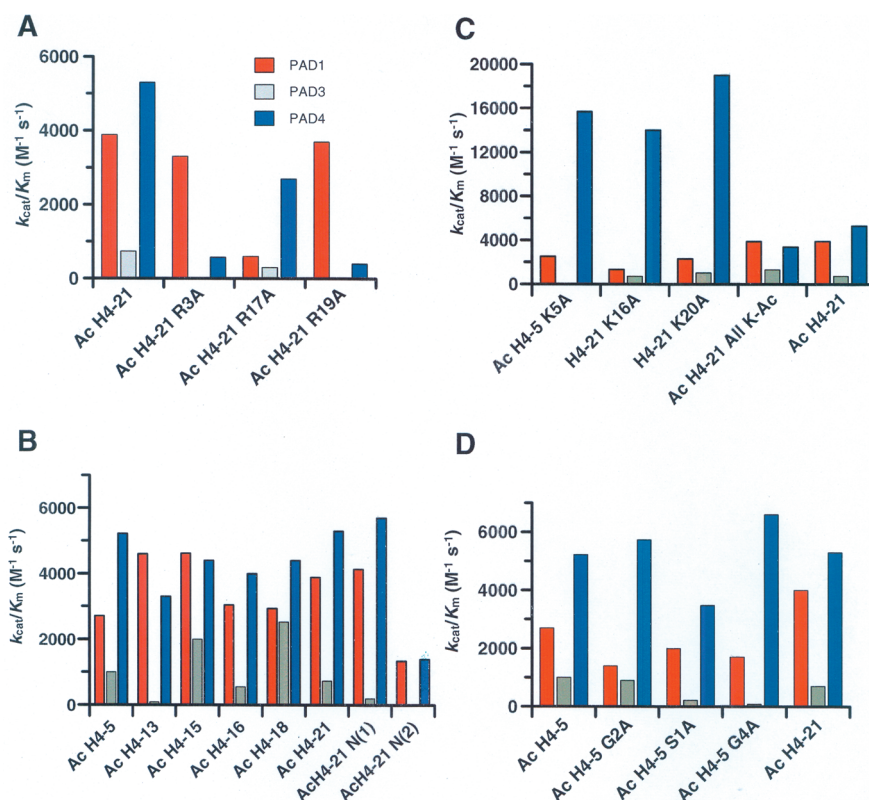
FIGURE 5: Plots of the k_{cat}/K_m data shown in Table 4 were generated to provide a visual depiction of the results of the substrate specificity studies on histone H4 tail mimics. Comparisons of the data to show (A) the major site of deimination as determined by Arg substitution, (B) the effects of peptide length on substrate recognition, and (C, D) the effects of site-directed "mutagenesis" experiments.

k_{cat}/K_m values for the AcH4−21 peptide and AcH4−21 all K-Ac peptide are very similar to one another, suggesting that a reduction in charge on residues that are near the sites of modification does not affect substrate binding. This result is consistent with the relatively minor effects observed when the neighboring Lys residues were converted to Ala (see above). For PAD3, the k_{cat}/K_m value for the AcH4−21 all K-Ac peptide increased by ∼2.5-fold, again suggesting that acetylation does not substantially affect substrate recognition. In contrast to the results for PADs 1 and 3, the k_{cat}/K_m for PAD4 with this peptide is reduced by ∼2-fold. Although this decrease would appear to contradict the results of the Lys → Ala substitutions, i.e., that positive charge diminishes substrate recognition, the increased steric bulk of the acetyl group may give rise to steric clashes that hinder substrate binding. Nevertheless, it should be noted that most of the effects on catalysis are relatively minor, suggesting that the presence or absence of positively charged residues near the site of modification has minimal effects on catalysis.

To evaluate the effects of residues directly adjacent to R3, we generated a series of peptides based on the sequence of the AcH4−5 peptide, in which each of the individual residues was mutated to Ala. Although the data did not reveal any major trends for either PADs 1 or 4, it is noteworthy that the AcH4−5 K5A peptide showed a greater than 3-fold increase in deiminating activity, as compared to the AcH4−5 peptide, again suggesting that a positive charge C-terminal to the site of modification is not preferred. In contrast, the data for PAD3 revealed several interesting findings. First, the k_{cat}/K_m for the AcH4−5 K5A peptide is reduced by ∼20-fold relative to the AcH4−5 peptide, suggesting that a positively charged residue at the R + 2 position is important for substrate recognition. Second, the fact that the replacement of Ser1 with an Ala residue reduces k_{cat}/K_m by

∼4.5-fold suggests that a hydrogen bond to the Ser hydroxyl contributes to substrate recognition. Third, greater conformational flexibility appears to be important for the binding of PAD3 to its substrates as the replacement of Gly4 with an Ala residue reduces k_{cat}/K_m by 12.5-fold; the greater flexibility of the AcH4−5 peptide may allow other residues, e.g., the substrate Arg or, alternatively, Lys5, to adopt a confirmation that is preferentially recognized by this enzyme (Table 4, Figure 5D).

Inhibition Experiments with F- and Cl-amidine. As described in the introduction, we have previously reported the design and synthesis of F- and Cl-amidine, which are the most potent PAD4 inhibitors described to date (*19, 25, 33*). To assess the selectivity of these compounds, and possibly gain insights that could guide the design of inhibitors with greater selectivity, we evaluated their ability to inhibit PADs 1 and 3. Initially, IC_{50} values were determined (Figure 6A, top panel). The values obtained for Cl-amidine were 0.8 ± 0.3 and 6.2 ± 1.0 μM for PADs 1 and 3, respectively. For PAD1, this represents an ∼5-fold increase in potency, whereas for PAD3, the value is roughly comparable to that obtained for PAD4. For F-amidine, the IC_{50} obtained with PAD1 (i.e., 29.5 ± 1.31 μM) is also quite similar to that obtained for PAD4 (i.e., 21.6 ± 2.10 μM (*25*)). Interestingly, the IC_{50} value obtained for F-amidine with PAD3 was significantly higher, i.e., ∼350 μM, than that obtained for either PAD1 or PAD4. These data suggest that Cl-amidine is a pan PAD inhibitor, whereas F-amidine is a PAD1/4 selective inhibitor. The possible reasons for the lack of F-amidine potency toward PAD3 are discussed below.

Inhibition by F-ethyl- and Cl-ethylamidine. The fact that the PAD3 k_{cat}/K_m value for BAEE is approximately 5-fold lower than that obtained for BAME (see above) suggested that it might be possible to generate an inhibitor that selectively inhibits PADs 1 and 4 over PAD3 by adding an ethyl group to the backbone
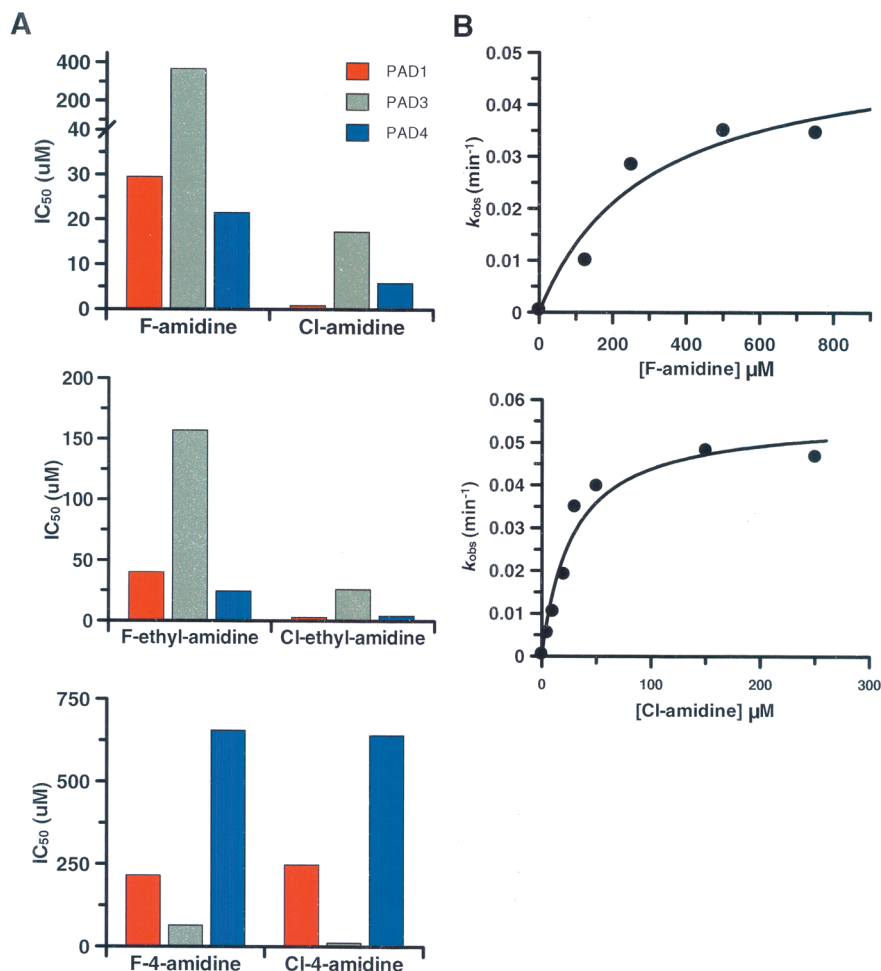
FIGURE 6: (A) Inhibition of PADs 1, 3, and 4 by (A) F- and Cl-amidine (top), F- and Cl-ethylamidine (middle), and F4- and Cl4-amidine (bottom). (B) Plot of k_{obs} versus the concentration of F-amidine (top) and Cl-amidine (bottom) for the inactivation of PAD3.

amide of F- and Cl-amidine. As such, F- and Cl-ethylamidine were synthesized (Figure 1B), and their ability to inhibit PADs 1, 3, and 4 was evaluated (Figure 6A, middle panel). The IC_{50} values of Cl-ethylamidine for PADs 1, 3, and 4 are 2.8 ± 0.3, 26 ± 4.6, and $4.1 \pm 1.7 \mu M$, respectively. The IC_{50} values of F-ethylamidine for PADs 1, 3, and 4 are 40 ± 19, 157 ± 58.0, and 24.3 ± 22.3, μM, respectively. Gratifyingly, the IC_{50} values for PADs 1 and 4 for both F-ethyl- and Cl-ethylamidine were quite similar to those obtained for F- and Cl-amidine. Somewhat surprisingly, however, the addition of the ethyl group did not lead to a significant improvement in inhibitor selectivity. The reasons for the lack of enhanced selectivity are unclear and require further investigation.

Inactivation of PAD3 by F- and Cl-amidine. We were intrigued by the large disparity in the inhibition constants obtained for PAD3 with F- and Cl-amidine and how these values compared to those obtained for PAD4. To gain insight into this disparity, we characterized the kinetics of PAD3 inactivation by both F- and Cl-amidine. Briefly, the pseudo-first-order rate constants of inactivation, i.e., k_{obs}, were obtained for various concentrations of inactivator at the pH optimum and subsequently plotted versus inactivator concentration. Because the plots are hyperbolic, an indication of a two-step mechanism of inactivation, the data were fit to eq 5 to obtain values for k_{inact}, K_I, and k_{inact}/K_I (Figure 6B). For F-amidine, these values are 0.05 ± 0.01 min^{-1}, $293 \pm 193 \mu M$, and 170 M^{-1} min^{-1}, respectively. Interestingly, the k_{inact}/K_I value is decreased > 15-fold relative to the previously reported value for PAD4 (*25*). This

decrease in k_{inact}/K_I is primarily due to a decrease in k_{inact} (~ 20-fold as compared to the previously reported value for PAD4 (*25*)). For Cl-amidine, the k_{inact} is 0.056 ± 0.005 min^{-1} and the K_I is $28 \pm 7.3 \mu M$, resulting in a k_{inact}/K_I of 2000 M^{-1} min^{-1} (Figure 6B). Relative to PAD4, these data indicate that k_{inact}/K_I is decreased by > 6-fold. Similarly to the results obtained for F-amidine, this decrease in k_{inact}/K_I is driven by a decrease in k_{inact} (~ 40-fold as compared to the previously reported value for PAD4 (*25*)).

The decrease in k_{inact} observed for both compounds with PAD3 is most easily explained by an inability to properly position the haloacetamidine warhead for nucleophilic attack by the active site Cys. To examine this possibility, we determined the IC_{50} values for derivatives of F- and Cl-amidine that incorporate a longer side chain; we reasoned that the longer side chain would allow for the proper positioning of the warhead for nucleophilic attack and would thus exhibit greater selectivity for PAD3. The structures of these compounds, denoted F4-amidine and Cl4-amidine, are depicted in Figure 1, and we have previously reported that they are relatively weak PAD4 inhibitors ($IC_{50} \geq 640 \mu M$) (*19*). The IC_{50} values are at least partially consistent with this hypothesis (Figure 6A, bottom panel). For example, the IC_{50} of F4-amidine for PAD3 was reduced by 5.7-fold, from 367 ± 189 to 64.4 ± 24.4 μM, whereas the IC_{50} values obtained for PADs 1 and 4 with this compound are increased by 270- and 30-fold, respectively. Although a less significant effect was observed with Cl4-amidine, the same trends emerge; Cl4-amidine shows > 20-fold and 50-fold selectivity for PAD3 over PAD1 and PAD4, respectively.

Thus, F4- and Cl4-amidine represent the first PAD3-selective inhibitors to be described in the literature, and they will undoubtedly serve as useful chemical probes to discern the physiological functions of this enzyme. It should be noted that dialysis experiments were used to demonstrate that these compounds irreversibly inactivate PAD3 (Supporting Information Figure S3).

SUMMARY

Dysregulated protein deimination is associated with the onset and progression of various diseases, most notably rheumatoid arthritis (RA) (*7, 56*). Several studies have identified PAD4 as the disease-implicated enzyme, and it has recently become a major target for the development of an RA therapeutic (*7*). In addition to PAD4, dysregulated PAD2 activity may also play a role in several diseases, including RA and multiple sclerosis (MS). Furthermore, the expression of PADs 2 and 4, as well as PADs 1 and 3, is known to overlap (*10*). Therefore, in order to discern the specific contributions of individual PAD isozymes to human disease, PAD-specific inhibitors are needed. In addition, such compounds will be useful for addressing the question of whether the inhibition of a single isozyme, or, alternatively, multiple isozymes, is required to treat these diseases. Finally, the development of PAD-selective inhibitors will undoubtedly provide powerful chemical tools that can be used to characterize the normal physiological roles of these enzymes.

To further aid in the development of isozyme-specific PAD inhibitors, we initiated studies on PADs 1 and 3, with the goal of identifying specific differences between isozymes that could be exploited for the development of such compounds. These studies revealed that, like PAD4, PADs 1 and 3 (i) are *bona fide* PADs, (ii) require supraphysiological concentrations of calcium for activity, similarly to previous reports (*32*), and (iii) utilize a reverse protonation mechanism. The results of substrate specificity studies also indicate that there are few PAD-specific recognition elements. For example, peptide length, acetylation status, and the presence or absence of charged residues proved, in most cases, to have only minor effects on the deiminating activity of PADs 1 and 4. The fact that peptide length has little influence on the deiminating activity of these isozymes is in stark contrast to other histone-modifying enzymes, e.g., protein arginine methyltransferase 1 (PRMT1), lysine-specific demethylase 1 (LSD1), and histone deacetylase 8 (HDAC8), where long-range interactions are critical for substrate recognition (*57−59*). The one exception is that longer range interactions do appear to contribute to PAD3 substrate recognition, and one key interaction appears to be the presence of a positively charged residue at the R + 2 position. This information will undoubtedly aid the future development of a PAD3-specific inhibitor. These studies have also shown that Cl-amidine and, to a lesser extent, F-amidine are pan PAD inhibitors and, more importantly, have led to the identification of F4- and Cl4-amidine as PAD3-selective inhibitors.

SUPPORTING INFORMATION AVAILABLE

Supplementary methods, Tables S1 and S2, and Figures S1−S3. This material is available free of charge via the Internet at http://pubs.acs.org.

REFERENCES

1. Schellekens, G. A., de Jong, B. A., van den Hoogen, F. H., van de Putte, L. B., and van Venrooij, W. J. (1998) Citrulline is an essential constituent of antigenic determinants recognized by rheumatoid arthritis-specific autoantibodies. *J. Clin. Invest. 101*, 273–281.
2. Moscarello, M. A., Mastronardi, F. G., and Wood, D. D. (2007) The role of citrullinated proteins suggests a novel mechanism in the pathogenesis of multiple sclerosis. *Neurochem. Res. 32*, 251–256.
3. Ishigami, A., Ohsawa, T., Hiratsuka, M., Taguchi, H., Kobayashi, S., Saito, Y., Murayama, S., Asaga, H., Toda, T., Kimura, N., and Maruyama, N. (2005) Abnormal accumulation of citrullinated proteins catalyzed by peptidylarginine deiminase in hippocampal extracts from patients with Alzheimer's disease. *J. Neurosci. Res. 80*, 120–128.
4. Chen, C. C., Isomoto, H., Narumi, Y., Sato, K., Oishi, Y., Kobayashi, T., Yanagihara, K., Mizuta, Y., Kohno, S., and Tsukamoto, K. (2008) Haplotypes of PADI4 susceptible to rheumatoid arthritis are also associated with ulcerative colitis in the Japanese population. *Clin. Immunol. 126*, 165–171.
5. Chang, X., Han, J., Pang, L., Zhao, Y., Yang, Y., and Shen, Z. (2009) Increased PADI4 expression in blood and tissues of patients with malignant tumors. *BMC Cancer 9*, 40.
6. Chang, X., and Han, J. (2006) Expression of peptidylarginine deiminase type 4 (PAD4) in various tumors. *Mol. Carcinog. 45*, 183–196.
7. Jones, J. E., Causey, C. P., Knuckley, B., Slack-Noyes, J. L., and Thompson, P. R. (2009) Protein arginine deiminase 4 (PAD4): Current understanding and future therapeutic potential. *Curr. Opin. Drug Discovery Dev. 12*, 616–627.
8. Kinloch, A., Lundberg, K., Wait, R., Wegner, N., Lim, N. H., Zendman, A. J., Saxne, T., Malmstrom, V., and Venables, P. J. (2008) Synovial fluid is a site of citrullination of autoantigens in inflammatory arthritis. *Arthritis Rheum. 58*, 2287–2295.
9. Chavanas, S., Mechin, M. C., Takahara, H., Kawada, A., Nachat, R., Serre, G., and Simon, M. (2004) Comparative analysis of the mouse and human peptidylarginine deiminase gene clusters reveals highly conserved non-coding segments and a new human gene, PADI6. *Gene 330*, 19–27.
10. Vossenaar, E. R., Zendman, A. J., van Venrooij, W. J., and Pruijn, G. J. (2003) PAD, a growing family of citrullinating enzymes: Genes, features and involvement in disease. *BioEssays 25*, 1106–1118.
11. Tarcsa, E., Marekov, L. N., Mei, G., Melino, G., Lee, S. C., and Steinert, P. M. (1996) Protein unfolding by peptidylarginine deiminase. Substrate specificity and structural relationships of the natural substrates trichohyalin and filaggrin. *J. Biol. Chem. 271*, 30709–30716.
12. Lee, Y. H., Coonrod, S. A., Kraus, W. L., Jelinek, M. A., and Stallcup, M. R. (2005) Regulation of coactivator complex assembly and function by protein arginine methylation and demethylimination. *Proc. Natl. Acad. Sci. U.S.A. 102*, 3611–3616.
13. Suzuki, A., Yamada, R., Chang, X., Tokuhiro, S., Sawada, T., Suzuki, M., Nagasaki, M., Nakayama-Hamada, M., Kawaida, R., Ono, M., Ohtsuki, M., Furukawa, H., Yoshino, S., Yukioka, M., Tohma, S., Matsubara, T., Wakitani, S., Teshima, R., Nishioka, Y., Sekine, A., Iida, A., Takahashi, A., Tsunoda, T., Nakamura, Y., and Yamamoto, K. (2003) Functional haplotypes of PADI4, encoding citrullinating enzyme peptidylarginine deiminase 4, are associated with rheumatoid arthritis. *Nat. Genet. 34*, 395–402.
14. Cuthbert, G. L., Daujat, S., Snowden, A. W., Erdjument-Bromage, H., Hagiwara, T., Yamada, M., Schneider, R., Gregory, P. D., Tempst, P., Bannister, A. J., and Kouzarides, T. (2004) Histone deimination antagonizes arginine methylation. *Cell 118*, 545–553.
15. Wang, Y., Wysocka, J., Sayegh, J., Lee, Y. H., Perlin, J. R., Leonelli, L., Sonbuchner, L. S., McDonald, C. H., Cook, R. G., Dou, Y., Roeder, R. G., Clarke, S., Stallcup, M. R., Allis, C. D., and Coonrod, S. A. (2004) Human PAD4 regulates histone arginine methylation levels via demethylimination. *Science 306*, 279–283.
16. Thompson, P. R., and Fast, W. (2006) Histone citrullination by protein arginine deiminase: Is arginine methylation a green light or a roadblock? *ACS Chem. Biol. 1*, 433–441.
17. Hagiwara, T., Hidaka, Y., and Yamada, M. (2005) Deimination of histone H2A and H4 at arginine 3 in HL-60 granulocytes. *Biochemistry 44*, 5827–5834.
18. Nakashima, K., Hagiwara, T., and Yamada, M. (2002) Nuclear localization of peptidylarginine deiminase V and histone deimination in granulocytes. *J. Biol. Chem. 277*, 49562–49568.
19. Luo, Y., Arita, K., Bhatia, M., Knuckley, B., Lee, Y. H., Stallcup, M. R., Sato, M., and Thompson, P. R. (2006) Inhibitors and inactivators of protein arginine deiminase 4: Functional and structural characterization. *Biochemistry 45*, 11727–11736.
20. Wang, J. S., and Chiu, Y. T. (2009) Systemic hypoxia enhances exercise-mediated bactericidal and subsequent apoptotic responses in human neutrophils, *J. Appl. Physiol.* (in press).
21. Neeli, I., Khan, S. N., and Radic, M. (2008) Histone deimination as a response to inflammatory stimuli in neutrophils. *J. Immunol. 180*, 1895–1902.

22. Asaga, H., Yamada, M., and Senshu, T. (1998) Selective deimination of vimentin in calcium ionophore-induced apoptosis of mouse peritoneal macrophages. *Biochem. Biophys. Res. Commun. 243*, 641–646.

23. Mizoguchi, M., Manabe, M., Kawamura, Y., Kondo, Y., Ishidoh, K., Kominami, E., Watanabe, K., Asaga, H., Senshu, T., and Ogawa, H. (1998) Deimination of 70-kD nuclear protein during epidermal apoptotic events in vitro. *J. Histochem. Cytochem. 46*, 1303–1309.

24. Wang, Y., Li, M., Stadler, S., Correll, S., Li, P., Wang, D., Hayama, R., Leonelli, L., Han, H., Grigoryev, S. A., Allis, C. D., and Coonrod, S. A. (2009) Histone hypercitrullination mediates chromatin decondensation and neutrophil extracellular trap formation. *J. Cell Biol. 184*, 205–213.

25. Luo, Y., Knuckley, B., Lee, Y. H., Stallcup, M. R., and Thompson, P. R. (2006) A fluoroacetamidine-based inactivator of protein arginine deiminase 4: Design, synthesis, and in vitro and in vivo evaluation. *J. Am. Chem. Soc. 128*, 1092–1093.

26. Knuckley, B., Causey, C. P., Pellechia, P. J., Cook, P. F., and Thompson, P. R. (2010) Haloacetamidine-based inactivators of protein arginine deiminase 4 (PAD4): Evidence that general acid catalysis promotes efficient inactivation. *ChemBioChem 11*, 161–165.

27. Nachat, R., Mechin, M. C., Takahara, H., Chavanas, S., Charveron, M., Serre, G., and Simon, M. (2005) Peptidylarginine deiminase isoforms 1−3 are expressed in the epidermis and involved in the deimination of K1 and filaggrin. *J. Invest. Dermatol. 124*, 384–393.

28. Nachat, R., Mechin, M. C., Charveron, M., Serre, G., Constans, J., and Simon, M. (2005) Peptidylarginine deiminase isoforms are differentially expressed in the anagen hair follicles and other human skin appendages. *J. Invest. Dermatol. 125*, 34–41.

29. Mechin, M. C., Sebbag, M., Arnaud, J., Nachat, R., Foulquier, C., Adoue, V., Coudane, F., Duplan, H., Schmitt, A. M., Chavanas, S., Guerrin, M., Serre, G., and Simon, M. (2007) Update on peptidylarginine deiminases and deimination in skin physiology and severe human diseases. *Int. J. Cosmet. Sci. 29*, 147–168.

30. Ishida-Yamamoto, A., Senshu, T., Takahashi, H., Akiyama, K., Nomura, K., and Iizuka, H. (2000) Decreased deiminated keratin K1 in psoriatic hyperproliferative epidermis. *J. Invest. Dermatol. 114*, 701–705.

31. Lu, J., Goldstein, K. M., Chen, P., Huang, S., Gelbert, L. M., and Nagpal, S. (2005) Transcriptional profiling of keratinocytes reveals a vitamin D-regulated epidermal differentiation network. *J. Invest. Dermatol. 124*, 778–785.

32. Kearney, P. L., Bhatia, M., Jones, N. G., Luo, Y., Glascock, M. C., Catchings, K. L., Yamada, M., and Thompson, P. R. (2005) Kinetic characterization of protein arginine deiminase 4: A transcriptional corepressor implicated in the onset and progression of rheumatoid arthritis. *Biochemistry 44*, 10570–10582.

33. Causey, C. P., and Thompson, P. R. (2008) An improved synthesis of haloacetamidine-based inactivators of protein arginine deiminase 4 (PAD4). *Tetrahedron Lett. 49*, 4383–4385.

34. Rus'd, A. A., Ikejiri, Y., Ono, H., Yonekawa, T., Shiraiwa, M., Kawada, A., and Takahara, H. (1999) Molecular cloning of cDNAs of mouse peptidylarginine deiminase type I, type III and type IV, and the expression pattern of type I in mouse. *Eur. J. Biochem. 259*, 660–669.

35. Zendman, A. J., Raijmakers, R., Nijenhuis, S., Vossenaar, E. R., Tillaart, M., Chirivi, R. G., Raats, J. M., van Venrooij, W. J., Drijfhout, J. W., and Pruijn, G. J. (2007) ABAP: Antibody-based assay for peptidylarginine deiminase activity. *Anal. Biochem. 369*, 232–240.

36. Knuckley, B., Bhatia, M., and Thompson, P. R. (2007) Protein arginine deiminase 4: Evidence for a reverse protonation mechanism. *Biochemistry 46*, 6578–6587.

37. Knipp, M., and Vasak, M. (2000) A colorimetric 96-well microtiter plate assay for the determination of enzymatically formed citrulline. *Anal. Biochem. 286*, 257–264.

38. Sugawara, K., and Oyama, F. (1981) Fluorogenic reaction and specific microdetermination of ammonia. *J. Biochem. 89*, 771–774.

39. Leatherbarrow, R. J. (2007) GraFit Version 6, 6.0 ed., Erithacus Software Limited, Horley, U.K.

40. Kearney, P. L., Bhatia, M., Jones, N. G., Yuan, L., Glascock, M. C., Catchings, K. L., Yamada, M., and Thompson, P. R. (2005) Kinetic characterization of protein arginine deiminase 4: A transcriptional corepressor implicated in the onset and progression of rheumatoid arthritis. *Biochemistry 44*, 10570–10582.

41. Mechin, M. C., Enji, M., Nachat, R., Chavanas, S., Charveron, M., Ishida-Yamamoto, A., Serre, G., Takahara, H., and Simon, M. (2005) The peptidylarginine deiminases expressed in human epidermis differ

in their substrate specificities and subcellular locations. *Cell. Mol. Life Sci. 62*, 1984–1995.

42. Nakayama-Hamada, M., Suzuki, A., Kubota, K., Takazawa, T., Ohsaka, M., Kawaida, R., Ono, M., Kasuya, A., Furukawa, H., Yamada, R., and Yamamoto, K. (2005) Comparison of enzymatic properties between hPADI2 and hPADI4. *Biochem. Biophys. Res. Commun. 327*, 192–200.

43. Musse, A. A., Polverini, E., Raijmakers, R., and Harauz, G. (2008) Kinetics of human peptidylarginine deiminase 2 (hPAD2)—Reduction of Ca^{2+} dependence by phospholipids and assessment of proposed inhibition by paclitaxel side chains. *Biochem. Cell Biol. 86*, 437–447.

44. Guerrin, M., Ishigami, A., Mechin, M. C., Nachat, R., Valmary, S., Sebbag, M., Simon, M., Senshu, T., and Serre, G. (2003) cDNA cloning, gene organization and expression analysis of human peptidylarginine deiminase type I. *Biochem. J. 370*, 167–174.

45. Arita, K., Hashimoto, H., Shimizu, T., Nakashima, K., Yamada, M., and Sato, M. (2004) Structural basis for Ca(2+)-induced activation of human PAD4. *Nat. Struct. Mol. Biol. 11*, 777–783.

46. Arita, K., Shimizu, T., Hashimoto, H., Hidaka, Y., Yamada, M., and Sato, M. (2006) Structural basis for histone N-terminal recognition by human peptidylarginine deiminase 4. *Proc. Natl. Acad. Sci. U.S.A. 103*, 5291–5296.

47. Knuckley, B., Bhatia, M., and Thompson, P. R. (2007) Protein arginine deiminase 4: Evidence for a reverse protonation mechanism. *Biochemistry 46*, 6578–6587.

48. Stone, E. M., Costello, A. L., Tierney, D. L., and Fast, W. (2006) Substrate-assisted cysteine deprotonation in the mechanism of dimethylargininase (DDAH) from *Pseudomonas aeruginosa*. *Biochemistry 45*, 5618–5630.

49. Lu, X., Li, L., Wu, R., Feng, X., Li, Z., Yang, H., Wang, C., Guo, H., Galkin, A., Herzberg, O., Mariano, P. S., Martin, B. M., and Dunaway-Mariano, D. (2006) Kinetic analysis of *Pseudomonas aeruginosa* arginine deiminase mutants and alternate substrates provides insight into structural determinants of function. *Biochemistry 45*, 1162–1172.

50. Li, L., Li, Z., Chen, D., Lu, X., Feng, X., Wright, E. C., Solberg, N. O., Dunaway-Mariano, D., Mariano, P. S., Galkin, A., Kulakova, L., Herzberg, O., Green-Church, K. B., and Zhang, L. (2008) Inactivation of microbial arginine deiminases by L-canavanine. *J. Am. Chem. Soc. 130*, 1918–1931.

51. Cleland, W. W. (1982) The use of pH studies to determine chemical mechanisms of enzyme-catalyzed reactions. *Methods Enzymol. 87*, 390–405.

52. Segel, I. H. (1975) Enzyme Kinetics: Behavior and Analysis of Rapid Equilibrium and Steady-State Enzyme Systems, Wiley-Interscience, New York.

53. Frankel, B. A., Kruger, R. G., Robinson, D. E., Kelleher, N. L., and McCafferty, D. G. (2005) *Staphylococcus aureus* sortase transpeptidase SrtA: Insight into the kinetic mechanism and evidence for a reverse protonation catalytic mechanism. *Biochemistry 44*, 11188–11200.

54. Asaga, H., Nakashima, K., Senshu, T., Ishigami, A., and Yamada, M. (2001) Immunocytochemical localization of peptidylarginine deiminase in human eosinophils and neutrophils. *J. Leukocyte Biol. 70*, 46–51.

55. Strahl, B. D., Briggs, S. D., Brame, C. J., Caldwell, J. A., Koh, S. S., Ma, H., Cook, R. G., Shabanowitz, J., Hunt, D. F., Stallcup, M. R., and Allis, C. D. (2001) Methylation of histone H4 at arginine 3 occurs in vivo and is mediated by the nuclear receptor coactivator PRMT1. *Curr. Biol. 11*, 996–1000.

56. Hill, J. A., Southwood, S., Sette, A., Jevnikar, A. M., Bell, D. A., and Cairns, E. (2003) Cutting edge: The conversion of arginine to citrulline allows for a high-affinity peptide interaction with the rheumatoid arthritis-associated HLA-DRB1*0401 MHC class II molecule. *J. Immunol. 171*, 538–541.

57. Osborne, T. C., Obianyo, O., Zhang, X., Cheng, X., and Thompson, P. R. (2007) Protein arginine methyltransferase 1: Positively charged residues in substrate peptides distal to the site of methylation are important for substrate binding and catalysis. *Biochemistry 46*, 13370–13381.

58. Gurard-Levin, Z. A., and Mrksich, M. (2008) The activity of HDAC8 depends on local and distal sequences of its peptide substrates. *Biochemistry 47*, 6242–6250.

59. Forneris, F., Binda, C., Vanoni, M. A., Battaglioli, E., and Mattevi, A. (2005) Human histone demethylase LSD1 reads the histone code. *J. Biol. Chem. 280*, 41360–41365.